Extraction of Organic Compounds from Representative Shales and the Effect on Porosity

Victoria H. DiStefano[1#], Joanna McFarlane[1], Lawrence M. Anovitz[1], Andrew G. Stack[1], Alexander D. Gordon[1], Ken C. Littrell[1], Steve J. Chipera[§], Rodney D. Hunt[1], Samuel A. Lewis[1], Sr., Richard E. Hale[1], Edmund Perfect[ξ]*

[1]Oak Ridge National Laboratory, Oak Ridge, TN

[#]Bredesen Center, University of Tennessee, Knoxville, TN

[§]Chesapeake Energy, Oklahoma City, OK

[ξ]Department of Earth and Planetary Science, University of Tennessee, Knoxville, TN

KEYWORDS small angle neutron scattering, solvent extraction from shales, Eagle Ford shale, Marcellus shale, pore size distribution.

---

[1] *This manuscript has been authored by UT-Battelle, LLC under Contract No. DE-AC05-00OR22725 with the U.S. Department of Energy. The United States Government retains and the publisher, by accepting the article for publication, acknowledges that the United States Government retains a non-exclusive, paid-up, irrevocable, world-wide license to publish or reproduce the published form of this manuscript, or allow others to do so, for United States Government purposes. The Department of Energy will provide public access to these results of federally sponsored research in accordance with the DOE Public Access Plan (http://energy.gov/downloads/doe-public-access-plan).*

ABSTRACT

As the location and accessibility of hydrocarbons is key to understanding and improving the extractability of hydrocarbons in hydraulic fracturing, this study is an attempt to understand how native organics are distributed with respect to pore size to determine the relationship between hydrocarbon chemistry and pore structure in shales. First, selected shale cores from the Eagle Ford and Marcellus formations were subjected to pyrolysis gas chromatography (GC), thermogravimetric analysis, and organic solvent extraction with the resulting effluent analyzed by GC-mass spectrometry (MS). Organics representing the oil and gas fraction (0.1 to 1 wt. %) were observed by GC-MS. For most of the samples, the amount of native organic extracted directly related to the percentage of clay in the shale. The porosity and pore size distribution (0.95 nm to 1.35 μm) in the Eagle Ford and Marcellus shales was measured before and after solvent extraction using small angle neutron scattering (SANS). An unconventional method was used to quantify the background from incoherent scattering as the Porod transformation obscures the Bragg peak from the clay minerals. The change in porosity from SANS is indicative of the extraction or breakdown of higher molecular weight bitumen with high C/H ratios (asphaltenes and resins). This is mostly likely attributed to complete dissolution or migration of asphaltenes and resins. These longer carbon chain lengths, C30-C40, were observed by pyrolysis GC, but either were too heavy to be analyzed in the extracts by GC-MS or were not effectively leached into the organic solvents. Thus, experimental limitations meant that the amount of extractable material could not be directly correlated to the changes in porosity measured by SANS. However, the observable porosity generally increased with solvent extraction. A decrease in porosity after extraction as observed in a shale with high clay content and low maturity was attributed to swelling of pores with solvent uptake or migration of resins and asphaltenes.

1. INTRODUCTION

During hydraulic fracturing, high-pressure fluids are used to improve the recovery of hydrocarbons from shales. These fluids break apart the shale and create pathways for hydrocarbons to escape. Without this fracturing, the low permeability of shales would prevent these resources from being economically recoverable. The efficiency of a fluid used to extract hydrocarbons is a complex function of fluid composition, accessible pore structure, and the location of hydrocarbons with respect to pore structure.(Weng, 2015) The type and nature of the organic matter present is also very important for oil and gas generation as the organic matter richness is indicative of the hydrocarbon generating potential of the source rock. Certain kerogen types indicate greater source-rock richness (thus greater hydrocarbon generating potential). (Huc, 2013)This study uses extraction with organic solvents in an attempt to understand how different portions of native organics are distributed within the shale, with respect to porosity. However, the goal of this work was not to replicate hydraulic fracturing or the fluids used in the process. Rather, the location and accessibility of bitumen with respect to pores, which is investigated in this work, is key to understanding and improving the extraction of hydrocarbons.

A thorough understanding of the porosity and pore size distribution in shales is critical to understanding what sizes, and in what proportion, pores are present before the stimulation of fractures by hydraulic fracturing. While studies have shown that the majority of porosity in shales is attributed to nanoporosity or pores below approximately 750 nm in diameter, (Loucks et al., 2009) it is not known whether pores at this scale are important in the storage and recovery of hydrocarbons. Studies to determine pore size distributions have used techniques such as low pressure gas adsorption with nitrogen (N_2) and carbon dioxide (CO_2) (Clarkson et al., 2013; Gu

et al., 2015; Kuila et al., 2014; Kuila et al., 2012; Mastalerz et al., 2013); mercury intrusion capillary pressure (Clarkson et al., 2013; Kuila et al., 2012; Mastalerz et al., 2013); low-field nuclear magnetic resonance (Ge et al., 2016; Rodriguez et al., 2014; Swainson, 2015; Webber et al., 2013); (Ultra) Small Angle X-ray Scattering ((U)SAXS), (Lee et al., 2014) and (Ultra) Small Angle Neutron Scattering ((U)SANS) (Anovitz et al., 2015; Clarkson et al., 2013; Gu et al., 2015; Swift et al., 2014; Wang et al., 2013); and scanning electron microscopy (SEM) (Chen et al., 2013). A more in depth review of these techniques can be found in Swainson (2015). Although each technique has its advantages and drawbacks, SANS is a non-destructive technique that allows pore structure to be maintained during the measurement, (Anovitz and Cole, 2015; Stack, 2015) generates data on the pore size distributions of connected and unconnected porosity from approximately 1 nm to 1 μm, and provides data on the surface roughness and interpore structure of relatively large rock samples. (Anovitz et al., 2015; Clarkson et al., 2013; Gu et al., 2015; Swift et al., 2014) Measured pore size distributions are needed for accurate models of hydrocarbon transport in shales.(Collell et al., 2015; Wang et al., 2016)

Nanopores in organic matter were first documented in the Barnett Shale, (Loucks et al., 2009) but have since been reported in most of the major gas producing shales worldwide, including the Eagle Ford and the Marcellus. (Anovitz et al., 2015; Bernard and Horsfield, 2014) This porosity may, in fact, form the interconnected three-dimensional network of pores required for extracting hydrocarbons. (Ambrose et al., 2010; Curtis et al., 2010; Sondergeld et al., 2010) The nanoporosity may both exist in the original rock, or may form from the exsolution of gaseous hydrocarbons during secondary cracking of oil. (Bernard et al., 2012a; Bernard et al., 2012b) In addition to the porosity in the organic matter, significant nanoporosity in shales has been measured in association with clay minerals.(Kuila and Prasad, 2013) The same group

identified three different types of porosity associated with tactoids, which are randomly oriented (i.e. turbostratic) stacks of clay mineral layers, and aggregates of tactoids: (1) 'Intra-tactoid' porosity associated with pore spaces about 3 nm in diameter within tactoids formed by the broken edges of the elementary clay layers in the tactoid stacks; (Aylmore and Quirk, 1971; Cases et al., 1992; Kuila and Prasad, 2013; Neaman et al., 2003) (2) 'Intertactoid' or 'intra-aggregate' porosity associated with pores about 50-100 nm in diameter within aggregates formed by the stacking of tactoids; and (3) 'Inter-aggregate' porosity associated with pores about 2 μm in diameter correlated with connections of pores between clay aggregates. Understanding the relationship of bitumen to nanopore structure, including pores found in organic matter and those associated with clays can, therefore, help elucidate where bitumen is stored in shale rock with respect to accessible porosity and pore size distribution, and how it may best be extracted.

In order to identify where native organic matter is stored in relation to accessible porosity in shales, SANS was used to determine pore size distributions before and after solvent extraction in samples of the Eagle Ford and Marcellus shales. Due to the heterogeneous nature of shales, pore size distribution and the type of extractable organic matter may be affected by a number of different parameters including lithology, maturity, and Total Organic Content (TOC). In order investigate correlations between rock composition–carbonate versus clay lithology, maturity, and the type of the hydrocarbons in the rocks, shale samples were selected with different provenance, mineralogy, and maturity. The extracted material was analyzed with GC-MS to determine the amount and type of extractable organics stored in the shales and which solvents were most effective in extracting organic matter. Shales were examined using thermogravimetric analysis (TGA) and pyrolysis gas chromatography-mass spectrometry (pGC-MS). The contacted samples

were also imaged using SEM before and after extraction to observe the contribution of larger scale (> 10 μm) porosity.

2. EXPERIMENTAL APPROACHES

2.1 Sample Origin and Preliminary Characterization

Shale core samples were obtained from the Eagle Ford (provided by Chesapeake Energy) and the Marcellus (purchased from Kocurek Industries) shale formations. Eagle Ford samples were recovered at depths (reported in Table 1a) and a detailed description of the location of these samples can be found elsewhere. (Anovitz et al., 2015) After recovery, Eagle Ford samples were wiped with dry kimwipes to remove any drilling fluids. These cores have very low permeability so little penetration of drilling muds into the bulk thickness is expected to have occurred. Marcellus cores were recovered from an outcrop. All cores were then vacuum-sealed in plastic and stored under ambient conditions until analysis. No treatment, such as oven-drying, was done prior to analysis. Each core was characterized using several techniques, including X-ray diffraction (XRD) to obtain mineralogy, by LECO TOC analysis to obtain total organic carbon (TOC), and pyrolysis in a Weatherford Source Rock Analyzer (SRA) to provide a measure of thermal maturity (R_0) and hydrogen index (HI). Based on the XRD and SRA analysis, the samples were grouped into a high thermal maturity group (carbonate- and clay-rich samples from the Eagle Ford, CARB HM, CLAY HM, and a sample from the Marcellus, MAR HM); and a low thermal maturity group from the Eagle Ford (CLAY LM, CARB LM). Micrographs before and after contact were obtained using SEM (Hitachi, S-3400N).

The shales were also analyzed by direct thermal treatment, monitoring the evolution of material by differential thermal analysis/thermogravimetric analysis (DTA/TGA) and by pyrolysis GC. A Harrop DTA/TGA was used to analyze 266 to 290 mg of ground sample from each core. The samples were heated in an Al_2O_3 crucible with an argon purge of 200 mL/min. The reference material was also Al_2O_3. Heat flux and mass were recorded simultaneously as the sample was heated from 50 to 600°C at a rate of 2.5 ° min^{-1}. The mass of unbound H_2O in the Eagle Ford samples was determined by gravimetry, independently from the TGA analysis, by heating unpulverized shale samples for 24 h at 105 °C. The shale samples were also analyzed by direct thermal desorption pyrolysis. The samples (50±5 mg) were prepared by grinding using a mortar and pestle before introduction into the pGC-MS instrument. The samples were rapidly heated from 40 to 350 °C in a Frontier Lab Multi-Shot Pyrolyzer, and the evolved material was passed through a Phenomenex ab-5 column and analyzed in a GC-MS (Agilent 7890A/5975) over mass range 40-700 amu. Release of lower molecular weight hydrocarbons and CO_2 could be measured with this technique, as compared with standard GC-MS methods.

2.2 Sample Preparation

For each core sample, six duplicate 1-mm-thick sections were cut perpendicular to bedding in successive concentric slices on a water-cooled rock saw. By cutting slices from a single core sample across the bedding, the inter-sample variability was limited so the uncontacted sample could be directly compared to the contacted samples. The samples were then briefly rinsed with ultrapure water (18.2 MΩ·cm) to remove any loose rock particles that may have adhered to the surface and allowed to dry overnight. After recording the mass, each of the

six duplicate sections was then either left untreated or leached in 10 mL of dichloromethane, toluene, hexane, acetone or methanol for 20 hours at 20°C (on a stir table), after which the shales were removed from the solvents and allowed to dry. Air drying is a very mild treatment and will not remove the clay-bound water from the samples. The presence of clay-bound water has been shown to decrease porosity (Lee et al., 2014); however, it would not have affected the change in porosity experienced by the samples during solvent extraction. A variety of solvents were selected to represent a range of properties, as given in Table 1. Whole sections and mild conditions were used for extraction to preserve the pore structure of the shale for SANS analysis, rather than more rigorous methods such as Soxhlet extraction.(Radke et al., 1978)

Table 1. Solvent Characteristics (Barton, 1983)

Solvent	Classification	Dipole Moment (D)	Solubility Parameter* $(MPa)^{0.5}$
acetone	polar aprotic	2.88	19.7
dichloromethane	non-polar	1.60	20.2
n-hexane	non-polar	0.00	14.9
n-dodecane	non-polar	0.00	16.0
methanol	polar protic	1.70	29.7
toluene	non-polar	0.36	18.3
water	polar protic	1.85	48.0

*Solubility parameters, or cohesive energy density, are calculated as heat of vaporization divided by molar volume. (Ballice and Larsen, 2003)

Sample mounts for SANS were prepared by Spectrum Petrographic, Inc. Each was mounted on a 1 mm thick quartz glass slide using epoxy and ground to approximately 150 microns. These thin sections of the shales were centered on an 8 mm mask for SANS analysis. Due to the low permeability of the samples, penetration by epoxy would be minor compared to section thickness and this method has been shown to result in negligible multiple scattering, as

well as limited scattering contributions from the slide and glue. (Anovitz et al., 2013; Anovitz et al., 2009)

2.3 Analysis of Extracts by Gas Chromatography

Hydrocarbons extracted from the shales were analyzed by gas chromatography using a Hewlett Packard (HP) 5890 gas chromatograph with a 5972 mass selective detector (MSD) running Enhanced ChemStation software (G1701BA version B.01.00). A DB5 capillary column (J&W Scientific) was used with ultrahigh purity (UHP) helium as a carrier gas (Air Liquide, 99.9999%) after passing through a desiccating column. Method details are given in Table 2. A solvent was run between each sample injection to minimize carryover of high molecular weight compounds, although these had negligible concentrations. Also, chromatograms during the hold at the highest temperature did not show evidence of the slow elution of high molecular weight compounds. Retention times were assigned based on the use of calibration runs and peak assignment was done using the ion fragmentation pattern from the GC-MS. The quantification uncertainty of the analyses was ±10% based on repeated measurements of calibration standards.

Table 2. GC-MSD Method

Component	*Settings*
Injector	250°C
	splitless
	2 or 10 µL
Detector	340°C
Column	DB5, 30 m length, 0.320 mm ID, 0.25µm film thickness
Solvent Delay	2.0 min
Carrier gas	UHP helium @ 4 bar
Oven Temperature Program	50-325°C @ 15°·min^{-1}
	Hold at 325°C for 3 min

Hydrocarbon elution times and sensitivities were determined using calibration standards, C6 through C28 and MA-EPH Aromatic Hydrocarbons (Absolute Standards Inc. Lots 030700 and 121399 respectively). Peak areas were normalized to the solvent peak, observed in the gas chromatograph. Sensitivity factors were calculated based on the signal from an internal standard, naphthalene *d-10*. Comparison between solvents for any particular shale, and comparisons between shales were calculated from chromatographic intensities at mass/charge, m/z = 57 relative to naphthalene. This $C_4H_9^+$ fragment appeared to account for most of the extractable hydrocarbon, although $C_6H_5^+$ (m/z = 77) was also observed in some chromatograms, particularly for toluene extractions. Calibration with absolute standards indicated that the volatility range of aromatic compounds that could be viewed directly would have ranged from naphthalene (retention time (RT) of 6.04 min) to benzoperylene (RT of 20.58 min) had they been present in the sample.

2.4 Analysis of Shales by Small Angle Neutron Scattering

The general purpose (GP)-SANS instrument at the ORNL High Flux Isotope Reactor (HFIR) was used to collect data on the porosity of the Eagle Ford shales before and after contact with organic solvents. The instrument can be used to study dense geological samples (Anovitz et al., 2013; Anovitz et al., 2009; Radliński, 2006; Radliński et al., 2004) because it takes advantage of the penetrating power of neutrons from the cold neutron source at HFIR, which interact with the nucleus of the atoms within the sample. (Wignall et al., 2012)

Spectra were obtained at three sample-to-detector distances (1.1 m, 7.8 m, and 18.3 m) to increase the observed angular range and, thus, the Q-range. The source radius was 20 mm and a

12 mm diameter sample mask was used for each sample-to-detector distance. The trap radii were 38 mm at 1.1 m and 7.8 m and 8mm at 18.3 m. The wavelengths of the neutrons were 4.75Å at 1.1 m and 7.8 m and 12 Å at 18.3 m with a wavelength spread $\Delta\lambda/\lambda = 0.15$. The resultant scattering vector ranged from 0.0003 to 0.7 $Å^{-1}$, which corresponds to sizes from approximately 9 to 20000 Å. Data were corrected for empty-beam scattering, background counts and detector uniformity, sample transmission and scattering volume, and reduced to absolute scale (differential cross-section per unit volume) by normalization to the intensity of the direct beam.

Our samples produced scattering patterns that were anisotropic with elliptical azimuthal symmetry, which has been documented in shales cut perpendicular to bedding. (Anovitz et al., 2015; Gu et al., 2015; Hall et al., 1986) However, anisotropy was not taken into account and scattering patterns were radially integrated over all scattering vectors, Q. This method has the effect of smoothing features in the pore size distribution, making peaks lower and broader than would have been observed if the data had been reduced considering anisotropy. (Swift et al., 2014)

2.4.1 Background Calculations

At high Q values, coherent (structural) scattering is overwhelmed by flat incoherent background scattering. (Swift et al., 2014) Traditionally, in shales and other rocks, the contribution of background scattering has been determined using a Porod transform, (Glatter and Kratky, 1982) which provides the background as the slope of a plot of Q^4I as a function of Q^4. However, the presence of ordered clays in these shale samples causes an interaction of incoherent scattering and clay Bragg peaks in the high Q-range, disrupting the background calculation from the Porod transform. (Kuila et al., 2014; Kuila and Prasad, 2013) The effect of

clay minerals in the high Q-range was also observed by Clarkson and colleagues. (Clarkson et al., 2013) In order not to obscure the effect of ordered clay minerals, the background was determined for each sample from the minimum intensity measured in the high Q-range. Since the background calculation relies on one point only, this increases uncertainty in the high Q-range (small pore sizes) SANS data, where background subtraction has the greatest effect on intensity.

2.4.2 Porosity Calculations

In SANS, scattering takes place at the interface of two adjacent phases. (Radliński and Hinde, 2002) The intensity of this scattering is determined by the square of the difference in the scattering length densities (SLDs) of these interfaces. (Anovitz et al., 2009; Radliński and Hinde, 2002; Swift et al., 2014) The largest difference in SLD in rocks occurs between minerals and pores, which leads to the two-phase approximation that allows porosity to be calculated from scattering curves. (Radliński and Hinde, 2002) Since the SLDs of light, aliphatic hydrocarbons, water, and empty pores are very similar, the porosity calculated from scattering curves includes empty pores and pores filled with water and aliphatic hydrocarbons (S1), here simply referred to as porosity. (Anovitz et al., 2015; Hall et al., 1986; Radliński and Hinde, 2002) As shown by Anovitz and colleagues (2015), SANS data can produce cumulative porosity as a function of pore diameters from about 1 nm to 1 μm. The porosity contribution at each pore diameter can be determined by step-wise subtraction from the cumulative porosity.

3. RESULTS

3.1 Characterization of Shale Cores

Lithology and maturity values obtained for each shale core sample are listed in Table 3a and Table 3b, respectively. In Table 3b, S1, S2, and S3 correspond to various fractions of the TOC in the samples calculated from the SRA pyrolysis. S1 refers to the free oil and gas that evolved from the sample, without the cracking of kerogen, at 300 ºC; S2 is the portion of hydrocarbons volatilized above 300 ºC that are released from the cracking of heavy hydrocarbons and from the thermal breakdown of kerogen; and S3 is the amount of CO_2 released from thermal cracking of kerogen. (McCarthy et al., 2011) The hydrogen and oxygen indices indicate that the kerogen present in the CARB LM and the CLAY LM samples are primarily Type I kerogen, which were most likely deposited in a lacustrine setting and is highly prone to generating oil and gas (~ 70-80% of the mass).(Huc, 2013) The very low hydrogen and oxygen indices in all of the high maturity samples indicate a thermally mature system where the distinction among kerogen type virtually disappears. (Huc, 2013)

Table 3a. Sample Lithology

Shale	Depth (m)	%Clay	%Carbonate	%Quartz	%Other	*%Illite/ Smectite
CARB HM	2415	4.0	85.4	6.5	4.1	2.4
CARB LM	1920	21.8	56.6	10.4	11.2	9.4
CLAY HM	2481	26.9	28.6	21.6	12.9	15.7
CLAY LM	1908	40.4	24.8	18.9	15.9	22.2
MAR HM	outcrop	35.2	12.1	44.1	8.6	18.6

* %Illite/Smectite refers to the percentage of mixed clay mineral in the shale.

Table 3b. Sample Maturity

Shale	Maturity (R_o)	TOC	Hydrogen Index	Oxygen Index	S1	S2	S3 (mg/g)	Production Index
CARB HM	1.57	0.50	107.07	28.28	0.68	0.53	0.14	0.562
CARB LM	0.58	6.58	555.32	4.86	6.07	36.54	0.32	0.142
CLAY HM	1.57	6.72	61.46	3.72	2.50	4.13	0.25	0.377
CLAY LM	0.58	3.76	529.79	6.12	5.16	19.92	0.23	0.206
MAR HM	1.60	4.31	6.03	3.71	0.05	0.26	0.16	0.161

The masses recorded before and after TGA analysis are given in Table 4, showing a range of mass losses from less than 1% to over 10%. The corresponding DTA traces did not give any indication of significant endothermic or exothermic reactive processes. TGA data were combined with rock evaluations, Table 3b, and independent measurements of unbound water content to indicate the fraction of hydrocarbons versus water mass loss coming from the shale. The structural water percentage was estimated by subtracting the other values from the overall mass loss. For all of the samples, the mass loss associated with water, either unbound or structural, was the major fraction present, occurring below 150 and above 400 °C respectively. The low maturity samples also indicated that S2 (kerogen breakdown above 300 °C) could have comprised a significant fraction of the mass loss in the TGA, in agreement with the Rock Eval analysis presented in Table 3b. The Eagle Ford and Marcellus high maturity samples had a comparatively small amount of organic released when heated to 600 °C, with the exception of the CLAY HM sample. The high mass loss shown at high temperatures is in agreement with the relatively high TOC observed in the Rock Eval analysis. Although, perhaps a counter-intuitive

finding for a high maturity sample, high TOC has been observed for other high clay composition shales, and relates to the lithography of the stratigraphic depth.

Table 4. Mass Loss from Thermogravimetric Analysis

Sample Identification	Initial Mass (mg) ±0.1 mg	Final Mass (mg) ±0.1 mg	Loss (wt. %) ±0.1%	Loss attributed to unbound H_2O (wt. %) ±0.4%
CARB HM	287.9	285.7	0.8	0.44
CARB LM	236.0	220.1	6.7	0.62
CLAY HM	289.3	259.6	10.3	0.80
CLAY LM	266.6	245.0	8.1	1.78
MAR HM	268.1	258.7	3.5	1.78

Pyrolysis GC analyses were performed to investigate differences in total hydrocarbon content between the different rock types and maturities, which could be compared with the analyzed extractable fractions. Classes of molecules desorbed are summarized in Table 5.

Table 5. Thermal Desorption Pyrolysis GC-MS

Sample Identification	Qualitative Analysis of Desorbed Species
CARB HM	paraffins up to high molecular weight, no CO_2
CARB LM	paraffins up to high molecular weight, butene, no parent polyaromatic hydrocarbons, little CO_2,
CLAY HM	paraffins, butene, CO_2, monoaromatics
CLAY LM	paraffins, branched as well as unbranched, CO_2 is lower
MAR HM	paraffins, CO_2, SO_2 (no H_2S)

Pyrolysis GC-MS chromatograms showed broad hydrocarbon distributions, with peak progressions typical of chain and branched paraffins. In addition to the C9-C28 progressions observed in the extracted material, paraffins of chain length C30-C40 were also observed in the samples. Small fragments such as butenes and light aromatic compounds were observed by pyrolysis GC-MS. However, the pyrolysis GC results showed no evidence of polyaromatic hydrocarbons at temperatures below 300°C. This suggests that larger molecular weight refractory material, if present, was not volatilized intact, but degradation of kerogen could have occurred at higher temperatures. The evaporative loss of light paraffins along with the higher temperature pyrolysis of aliphatic and aromatic compounds in the heating of shales has been reported elsewhere. (Ballice and Larsen, 2003)

CO_2 was also observed from the pyrolysis GC-MS of the samples analyzed. However, this was not correlated with carbonate in the shale. No CO_2 was evolved from the carbonate-rich sample CARB HM, while the most CO_2 came from CLAY HM, a clay-rich shale. As temperatures in the pyrolysis GC-MS were not high enough to decompose the carbonate minerals, the evolved CO_2 likely arose from the breakdown of organic matter.

3.2 Gas Chromatography of Solvent Fluids

Gas chromatograms for the solvent extractions from the shales are shown in Fig. 1. Data are plotted for $C_4H_9^+$, but are similar in appearance to the total ion chromatogram. The chromatogram retention times are characteristic of carbon chain lengths between C9-C28. Lighter hydrocarbons were not detectable in the chromatogram as they were obscured by the solvent peak. Hydrocarbons larger than C28 (boiling point = 432 °C), would not have passed through the column.

The solubilized material had little aromatic character. The paraffinic progression seen in the pyrolysis GC-MS was also observed in the chromatograms of extracted organics, although the chromatograms differed because in the former case the hydrocarbons came from thermal desorption and in the latter they came from solvent extraction. The ion chromatograms corresponding to the phenyl radical ($C_6H_5^+$), showed very low signal-to-noise ratios. Primarily the toluene extractions, but also the dichloromethane, contacts exhibited a large peak that evolved between 15 and 16 minutes with an aromatic signature with $C_6H_5^+$. The peak was not present in the toluene solvent and eluted much later than toluene, the latter (m/z = 91) seen at 3.101 min. Other masses associated with this peak include m/z = 105 and 57 as well as the sum of these at m/z = 163. Butene radical ($C_3H_4^+$, m/z = 51) was also present, corroborating pyrolysis GC-MS results. These peaks may have come from the fragmentation of a phenolic ketone evolved from the degradation of resins in the shale. (Kemp, 1981)

Quantifications of the total ion chromatograms from GC-MS of the extracted hydrocarbons are shown in Figs. 2 and 3. The relative amounts of material extracted were calculated based on normalization procedures discussed in section 2.3. Hence, the intensity of the chromatograms corresponds to the efficiency of the solvent in extracting hydrocarbons from the shale. In the case of CARB HM, the high-maturity carbonate-rich shale, all of the solvents performed similarly, and a single broad hump was observed in the chromatogram peaking at about 13-14 min retention time (Fig. 1a). Leachate chromatograms from CLAY HM, the high-maturity clay-rich shale (Fig. 1c), showed a significant early elution of lighter hydrocarbons as would be expected from a more mature formation. Toluene and hexane acted effectively in extracting material from this shale, corroborated by pyrolysis GC-MS in the observation of lighter aromatics. The two low maturity Eagle Ford shales, CARB LM and CLAY LM, had

similar broad peaks in hydrocarbon distribution at 16 to 17 min (Figs. 1b and 1d respectively), but CARB LM also had a significant extraction at lower masses, with a broad peak at 12 min. Non-polar solvents, hexane and dichloromethane, worked particularly well in extracting organic matter from these shales, although toluene was also able to remove a significant amount of material. None of the solvents worked well for the Marcellus shale, although a broad distribution of paraffins was observed in the effluent at longer retention times, at 18 min (Fig. 1e).

3.3 SANS Results

Cumulative porosities measured by SANS before and after extraction, are presented in Table 6, with the total change in porosity in italics. The cumulative porosity curves obtained from SANS were also analyzed to produce plots of pore size distributions for each sample exposed to the various solvents (Fig. 4). These plots show how the porosity distribution of each sample changes as a function of pore size diameter over the range of approximately 1 nm to 1 μm, after contact with each solvent. The International Union of Pure and Applied Chemistry recommend a classification of pores in the nanoporosity range according to the diameter of their pore size; (Sing et al., 1985) however, this classification is not always appropriate for shales and, in the case of our samples, may obscures important features observed in the pore size distribution plots. (Kuila and Prasad, 2013) Consequently, ranges of pore sizes were identified in the pore size distribution plots as ranges of interest based on the distribution of peaks and artifacts of changing detector distances (Table 7). In each of these ranges, the total change in porosity for each of the contacted samples (with respect to the uncontacted samples) was calculated. In order to account for the different sizes of the ranges, the change in porosity was then normalized to the porosity of the uncontacted samples by subtracting the extracted porosity by the initial porosity then

dividing by the initial porosity (Fig. 5). Ranges 1 and 2 (pores below 8.91 nm in diameter) were the most affected by uncertainties associated with background subtraction and had the largest changes in porosity, thus, they are not presented in Fig. 6.

Table 6. Porosities measured by SANS for shales before and after contact with solvents

Cumulative Porosity (%), (uncertainty), and *Change in Porosity (%)*						
Sample	**Before Contact**	**Dichloromethane**	**Acetone**	**Hexanes**	**Methanol**	**Toluene**
CARB HM	2.22 (0.18)	2.24 (0.17)	2.31 (0.16)	2.49 (0.22)	2.36 (0.15)	2.69 (0.20)
Change		*0.02*	*0.09*	*0.27*	*0.14*	*0.47*
CARB LM	8.15 (1.18)	9.41 (1.45)	10.50	10.43 (1.74)	10.50 (1.80)	9.91 (1.70)
Change		*1.26*	(1.66) *2.35*	*2.28*	*2.35*	*1.76*
CLAY HM	8.19 (1.62)	8.44 (1.59)	8.59 (1.63)	7.57 (1.46)	7.84 (1.45)	8.57 (1.78)
Change		*0.25*	*0.40*	*-0.62*	*-0.36*	*0.37*
CLAY LM	8.88 (1.85)	5.21 (1.00)	8.48 (2.06)	8.44 (2.00)	6.28 (1.39)	4.77 (1.00)
Change		*-3.67*	*-0.41*	*-0.45*	*-2.60*	*-4.11*
MAR HM	4.02 (1.01)	5.49 (1.28)	6.50 (1.09)	6.21 (1.32)	6.84 (1.14)	6.05 (1.58)
Change		*1.47*	*2.48*	*2.19*	*2.82*	*2.03*

Table 7. Pore Size Ranges for SANS Analysis

Ranges	**Pore Diameter (Å)**	**Pore Diameter (nm)**
1	9.54 – 16.69	0.95 – 1.67
2	16.69 – 89.06	1.67 – 8.91
3	89.06 – 585.97	8.91 – 58.60
4	585.97 –2719.84	58.60 – 271.98
5	2719.84– 13,536.7	271.98 – 1,353.67

4. DISCUSSION

4.1 Gas Chromatography of the Effluent and the Shale

Gas chromatographic analyses of the solvent extraction of native organics from shales are summarized in Figs. 2 and 3. Fig. 2 shows the mass fraction of hydrocarbons extracted by each of the five solvents from each shale sample, and Fig. 3 shows the mass of hydrocarbons extracted. As expected, the most effective solvents have representative characteristics, such as the solubility parameter and dipole moment (Table 1) that best match those of the native organics in the shales. Polar solvents, such as methanol and acetone, did not extract as much material as did non-polar solvents such as toluene, dichloromethane and hexane, except for in CARB HM where acetone removed the most material. While there was a large variation in the amount of organic material extracted with acetone, the amount removed with the methanol was relatively similar for all five samples.

Results for the low TOC Eagle Ford shale, CARB HM, were quantitatively and qualitatively different from the other Eagle Ford samples. The amount extracted was very low, and acetone and methanol both had a relatively high loading of hydrocarbons. The small amount extracted (Fig. 3) is consistent with the relatively small TOC value for CARB HM relative to the other Eagle Ford samples. The mass spectrum of the extracted material also indicates the presence of an aliphatic ketone, which was not seen in extractions from the other shales and is likely an artifact of external contamination.

The distribution of chain lengths in the extracted hydrocarbons is expected to change as the shale matures, producing both lighter and heavier fragments during metagenesis. This was, in fact, observed in the profiles of GC-MS paraffinic hydrocarbons extracted from these shale samples (Fig. 1). The amount of material extracted from the higher maturity shales was less than

that extracted from the lower maturity samples, consistent with the production of more refractory material during maturation. In the pyrolysis GC results for the clay-rich samples, the hydrocarbon envelope for the higher maturity sample shifted to earlier retention times (lower molecular weight) relative to that of the lower maturity sample. The shift is not apparent for the carbonate-rich shales. Quantification of the pyrolysis GC-MS results confirms that more C7-C28 is available from the samples with a significant percentage of clay, and more hydrocarbons are extracted from less-mature formations. In addition, significant C30-C40 was observed in the pyrolysis GC of the CARB LM and MAR HM samples.

The extraction pattern from the Marcellus shale was significantly different from that from the Eagle Ford (Fig. 1). Even though the TOC value of the Marcellus sample was comparable (4.31 %, Table 2) the amount dissolved in the non-polar solvents was much lower than in the Eagle Ford samples, and had a different chemical profile. The GC results showed that most of the material extracted was removed by toluene and dichloromethane and extraction by hexane was negligible. While most solvents only extracted small amounts in the Marcellus, methanol was approximately as effective as in the Eagle Ford samples (Fig. 3). Thermal analysis of the Marcellus also indicates that the hydrocarbons are tightly bound, as most of the mass loss could be attributed to H_2O, either bound or unbound, similar to the pattern observed with the high maturity Eagle Ford samples.

4.2 Porosity and Pore Size Distributions in the Shales

Cumulative porosities presented in Table 6 represent the porosity from ranges 2 through 5 (~2 nm – 1.4 μm). Range 1 (< 1.7 nm) was not included in the cumulative porosity calculation because of the large uncertainty associated with background subtraction at the smallest pore

sizes. (Bahadur et al., 2015) Additionally, since range 2 (1.7 – 8.9 nm) was also significantly affected by background subtraction, the contribution to porosity from range 2 is taken as the uncertainty in the cumulative porosity, presented in parenthesis. The cumulative porosities of the uncontacted samples shown in Table 6 are lower than the anisotropic porosity values reported earlier (Anovitz et al., 2015) on the same shale cores. While some of this difference could be due to sample heterogeneity, most can be attributed to the larger range of pore sizes capable of being observed by using USANS in the earlier study. (Anovitz et al., 2015) Total porosity values presented in Table 6 are thus conservative estimates and are expected to be much higher if porosity contributions outside the observed range are considered.

In the uncontacted samples, there was a notable trend in cumulative porosity with maturity. In the carbonate-rich Eagle Ford samples the lower maturity sample had much higher porosity than the higher maturity sample. This trend was also observed, to a lesser extent, in the clay-rich samples, however the slight difference in porosity was within the error calculated for these samples. This trend with maturity is consistent with trends of porosity versus maturity reported earlier on the same shale cores (Anovitz et al., 2015), as well as on different shales studied elsewhere. (Bahadur et al., 2015; Mastalerz et al., 2013)

The pore size distributions in most of the samples, including the extracted samples (Fig. 5), show a bimodal distribution in ranges 2 through 5 (1.67 nm – 1.35 μm). This bimodal distribution has been reported elsewhere when looking at pore ranges from approximately 1.7 to 200 nm in shales. (Clarkson et al., 2013; Kuila et al., 2014; Swift et al., 2014) The maxima of the distributions in our samples occur at about 2.72 nm in range 2 (1.7 – 8.9 nm) and around 500 to 800 nm, depending upon the sample, in range 5 (272 nm to 1.35 μm).

The peak in range 2 has been observed in other shale studies using methods besides SANS, and is commonly attributed to pores caused by clay structure, specifically intra-tactoid porosity. (Kuila and Prasad, 2013) The traditional method of background subtraction for SANS, using the Porod plot, obscures this peak. However, by using the minimum intensity as background, this peak can be observed in most of the samples examined. While the use of a single datum to approximate the background increases the uncertainty in our results, that the peak in range 2 is consistently present among the various solvents and across samples lends validity to this method of background subtraction. The results also suggest that the total porosity contribution from the peak in range 2 is generally proportional to the percentage of clay in the sample (Fig. 6). For example, CARB HM has the lowest clay content (4.0 %) and the smallest peak in range 2. This supports earlier findings that this peak is associated with clay porosity. (Kuila and Prasad, 2013)

In other studies on pore size distribution in shale, a maximum at larger pore sizes is observed, but the pore diameter at which it occurs varies. For example, Kuila and Prasad (2013) observed maxima at 50-100 nm and 2 μm which they attributed to intertactoid and inter-aggregate porosity, respectively. However, in our samples the peak occurred in the 272 nm to 1.35 μm range suggesting that these samples contained larger clay aggregates, creating larger pores, or that the porosity observed by this peak is not associated with clays and could be associated with porous organic matter. Whatever the cause, these larger pore structures contributed greatly to the porosity, more than size range 2 in most of the samples.

The pore size distribution below about 2 nm (range 1) also shows a distinctive peak around about 1 nm and contributes greatly to the total porosity of the sample. This peak, however, is usually defined by only one or two data points and is the range most affected by

background subtraction. Therefore, any conclusions about porosity at this scale are tenuous and require further investigation.

4.3 Comparison of Gas Chromatography and SANS Results

Although it is clear that dissolution of organic matter must change the pore structure of shales, it is difficult to correlate the porosity changes observed in SANS after solvent extraction with the amount of material extracted as measured by GS-MS. This is because porosity changes in SANS are attributed to the breakdown of the larger organics with higher C/H ratios, such as the resins and asphaltenes in bitumen (Radliński et al., 2000; Radliński and Hinde, 2002), while the GC-MS data show mainly aliphatic hydrocarbons up to C28. Nonetheless, the effects of solvent contact can be analyzed using the SANS technique, and our results suggest that they show a significant, measureable effect on the porosity distribution, discussed below. Our results further suggest that this effect is not universal, but depends on specific characteristics of both the shale and the solvent.

4.3.1 Chemical Interactions and Extraction

As discussed in 2.4.2, the creation of empty pores due to the removal of aliphatic hydrocarbons (S1 organic matter) by solvent dissolution should not significantly change the porosity observed in a SANS experiment, because pores filled with aliphatics and empty pores contribute almost equally to scattering. (Radliński and Hinde, 2002) Observed changes in porosity can instead be attributed to the removal or breakdown of resins and asphaltenes in bitumen, also known as the S2 organic portion. These have SLDs closer to that of the

surrounding matrix, and thus their removal will increase the scattering intensity by increasing the scattering contrast between the pore and its matrix (Fig. 7).

Based on this analysis, our results clearly suggest that resins and asphaltenes have been dissolved from pores at all scales observed. This is supported by the fact that there is a positive correlation in the initial amount of S2 (hydrocarbons volatilized above 300 ºC) in each sample and measured increases in porosity calculated from SANS, which is less distinct for other portions of organic matter (TOC, S1, and S3). This removal can occur in pores through three possible mechanisms (Fig. 7); 1) the complete breakdown of porous resins or asphaltenes, 2) dissolution and migration of resins and asphaltenes (cf. discussion of the effects of maturation by Radliński (Radliński et al., 2000) or 3) the partial dissolution of the organic matter, forming smaller pores within the organic matter. The first and second mechanisms lead to an increase and decrease, respectively, in scattering intensity in the pores at all scales. In the second mechanism, the migration of heavier organic material (higher SLD) scatters less at matrix boundaries than previously empty or water-filled pores. (Radliński et al., 2000) As shown by Rother and coworkers, (Rother et al., 2007) the third mechanism will lead to the formation of a smaller set of pores, or at least shift the pore-size distribution.

Our data suggest that Mechanism 1 or 2, or a combination of the two, is most likely dominant. This is because no shift in the pore size distribution peaks was observed with solvent extraction in any of the samples. However, the increase in porosity observed with scattering in most of the samples (CARB HM, CARB LM, CLAY HM, and MAR HM) are most likely attributed to Mechanism 1 and the decrease in porosity in CLAY LM to Mechanism 2.

When considering the change in cumulative porosity (Table 6) the higher maturity Eagle Ford samples (CARB HM and CLAY HM) showed very little observable change in porosity

arising from extraction, while the lower maturity Eagle Ford samples showed much greater changes, with the measured porosity of CARB LM generally increasing and that of CLAY LM generally decreasing. The high maturity Marcellus sample (MAR HM) also showed an increase in porosity. These trends are discussed in more detail below.

The changes in porosity with extraction, normalized to the initial porosity of each sample, are shown in Fig. 5. There are two possible explanations for the differences between the magnitude of the changes in the high-and low-maturity samples, solvent penetration or the amount of extractable material. For the Eagle Ford samples, both mechanisms are possible. The greater change in porosity in the low-maturity compared to the higher-maturity samples in the Eagle Ford could be due to greater penetration of solvent into the sample during extraction. Additionally, the lower maturity samples have larger S2 values, and thus more extractable material. Although, the Marcellus sample (MAR HM) was a high maturity sample, the increases in porosity were very large (from about 30 to 160 %), perhaps indicating greater solvent penetration.

Most of the samples showed an increase in porosity with extraction, which is expected when native organics are removed from the shales. However, the CLAY LM sample showed a large *decrease* in porosity with extraction which was unexpected. This may be the result of physical interactions between the clays and organic solvents, such as clay swelling. These are discussed in more detail in section 4.3.2. It could also reflect partial dissolution and transport of fairly mature organics into previously empty pores, as per Mechanism 2 above.

Interestingly, the magnitude of the porosity change in the larger pore sizes (ranges 3 through 5; pores > 8.9 nm) was relatively consistent across the various ranges for each solvent. This was not true for the smaller pore sizes (ranges 1 and 2; pores < 8.9 nm). While the porosity

522 contribution from ranges 1 and 2 are difficult to assess due to uncertainties caused by
523 background subtraction; the trends are very different from those in ranges 3 through 5. A
524 decrease in porosity in range 1, especially in solvent contacted CARB LM, CLAY HM, and
525 MAR HM, supports Mechanism 1 of pore formation through the obliteration of nanoporous
526 bitumen (Fig. 7).

527 4.3.2 Physical interaction of clays and organic solvents

528 In addition to the chemical interactions between the clays and native organic matter and
529 the solvents described above, physical processes may also have affected the pore structure of the
530 shales. The interaction of organic solvents with clay minerals has been reviewed by Kowlska,
531 Güler, and Cocke. (Kowalska et al., 1994) Solvents can interact directly with clay minerals
532 through van der Waals or Lewis acid-base forces, resulting in adsorption of the organic onto the
533 clay. The polar interactions are governed by the electron donor or acceptor properties of the clays
534 and the solvents, often corresponding to the hydrogen bonding ability of the materials. (Cervini-
535 Silva, 2004) Properties of the solvent that affect bonding are its hydrophobicity, the presence of
536 electronegative groups and pi bonds, molecular weight, and chain length.

537 Smectitic clays are hydrophilic, allowing water to penetrate between the negatively
538 charged clay layers causing swelling. Water solvates the cations located between the mineral
539 layers and adhered to external clay surfaces. The intercalated water affects electron transfer
540 processes by coordinating with metallic cations, and hence may impede the interactions of clays
541 with organic solvents. (Yariv, 1996) Introduction of solvents, particularly those that can accept a
542 proton from bound water molecules, changes the energetics of that interaction. Organic solvents
543 may also wet the interfacial surfaces, but their penetration may be impeded by pockets of more
544 tightly bound water. (Warren et al., 1986) In our experiments, the extracted amount of native

organic matter correlated directly with the amount of the clay, as shown in Fig. 3. Mixed illite/smectite clays dominate the samples analyzed, but because of the similarity in illite-to-smectite ratios for all the Eagle Ford samples, the amount extracted also corresponds to the percentage of expandable smectite layers.

The oil and gas industry uses CO_2-toluene cleaners on reservoir rocks, cycling through numerous times, with the intent of removing oil that is blocking the pores to get a true permeability. Like many of the methods in the industry, this has been extended from conventional reservoir rocks, such as sandstones and carbonates, to unconventional shale reservoirs with much lower porosity and permeability. Shale behaves differently than other reservoir rocks and has demonstrated interesting results that are not fully explained, including a decrease in permeability after CO_2-toluene cleaning. This decrease may be attributed to kerogen swelling due to the toluene. Another example of solvent interactions, this time with manufactured clays, has been shown to depend on the solvent having both hydrophobic and hydrophilic groups. (Jones, 1983) Pure hydrocarbons, such as hexane, are not as effective at penetrating layers in the clay as polar solvents, because the energetics of intercalation are not favorable. Polar, aromatic, and hydrogen bonding solvents can form stable complexes in the interlayer spaces, causing swelling of the clay matrix.

In the experiments report here, the increase in porosity did not correlate directly with dipole moment, similar to what was reported by Jones (1983). For instance, acetone had a comparatively small effect on porosity in the CLAY LM sample relative to methanol and DCM. The high dipole moment of acetone, 2.88, may have made access of acetone into the clay matrix much more difficult than methanol and DCM, with dipole moments of 1.7 and 1.6 respectively. Graber and Mingelgrin modeled the swelling of clays using regular solution theory. They found

that the greatest effect was for solvents having a solubility parameter closest to the clay matrix, similar to the effect seen in polymeric systems. (Graber and Mingelgrin, 1994) Thus the literature supports the hypothesis that in the experiments reported here the solvents caused swelling in the clays by interaction with the kerogen and bitumen in the pores.

In the MAR HM and CARB LM samples, polar methanol and acetone increased the porosity observed by SANS in range 5 (272 nm to 1.35 μm) more than the other solvents. While acetone and methanol extractions yielded a significant change in porosity in the Marcellus sample, relatively little paraffinic extraction was observed by GC-MS. MAR HM and CARB LM contain more longer-chain organic matter, C30 to C40 (observed by pGC-MS), present only in smaller amounts in the other samples. This organic matter would not have been observed by GC-MS in the extraction effluent, but removal or breakdown would have been observed as increased porosity in SANS. Methanol in particular has been observed to penetrate and attack larger organics and convert them into smaller, extractable molecules. (Koel et al., 2001) The increase in porosity after methanol contact in range 5 (pores > 270 nm) could, therefore, indicate deposits of larger asphaltenes and resins with polar groups (Fig. 7, Mechanism 1), or the scale of pore created during solvent induced breakdown of even larger pockets of organic matter (Fig. 7, Mechanism 2 or 3). Alternatively, the increase in porosity at this scale could be attributed to displacement of water in the interlayer spacings and subsequent dehydration of clays. Solvent uptake into porous materials through displacement of water can cause evaporative drying, (Kabiri and Zohuriaan-Mehr, 2004; Saliger et al., 1997) and has been found to shrink smaller pores (less than 6 Å) and enlarge larger pores. (Job et al., 2005) Although shales may experience evaporative drying, in none of the samples was a shift observed in the pore volume distribution

maxima, suggesting that drying was not an important mechanism in these shale-solvent interactions.

The sample CLAY LM is unique amongst the samples analyzed here in that its porosity decreased significantly in the solvent extracted samples relative to the starting material. Scanning electron microscope images of CLAY LM (Fig. 8) show that fissures in the rock that existed before extraction appear to have sealed after contact with dichloromethane possibly due to swelling of the clays from exposure to the solvent. CLAY LM also had the greatest percentage of clay minerals (40.4 %), including Illite/Smectite (22.2 %). The extent of the decrease observed by SANS varies, however, from solvent to solvent. Although interlayer water molecules in smectites can be displaced by solvents, this is primarily true for small polar organics such as methanol that can form hydrogen bonds with mineral surfaces. (Lagaly, 1984) Hydrogen bonding solvents (such as methanol) have been reported to swell clays more than polar aprotic (acetone) and non-polar solvents. (Job et al., 2005) Therefore, a larger decrease in porosity would be expected with polar than non-polar solvents. This is partially consistent with our results for CLAY LM, in which methanol (polar), for example, decreased porosity more in than did hexane (non-polar). However, non-polar toluene and weakly polar dichloromethane decreased porosity more even than did methanol suggesting that, for these solvents, chemical interactions with the organic materials were more important than physical swelling of the clays (see Section 4.3.1).

5. CONCLUSIONS

In this study, we used neutron scattering to complement conventional methods of geochemical analysis to investigate the link between the type of extractable organic material

present in shales and the porosity (or pore size distribution) of the rock. Our goal was to understand the nature and location of hydrocarbons in these shales. For most of the samples, the amount of native organic extracted, representative of the oil fraction, directly relates to the percentage of clay in the shale. Toluene, dichloromethane, and hexane were the best solvents for extraction, because they are chemically compatible with the paraffinic hydrocarbons in the shales.

Differences in SANS data before and after leaching indicated, as expected, that extractions change cumulative porosity. Changes in the porosity calculated by SANS are indicative of the extraction or breakdown of higher molecular weight bitumen with higher C/H ratios (asphaltenes and resins), which compose the S2 portion of TOC. This can occur though at least three mechanisms (Fig. 7); the complete dissolution of asphaltenes and resins (Mechanism 1), the extraction and migration of asphaltenes and resins, which get trapped in the pore matrix (Mechanism 2), or the partial breakdown of refractory organic matter, creating smaller pores (Mechanism 3). Larger molecules could not be observed in the GC-MS of the effluent, but hydrocarbons up to C40 were observed in the pyrolysis GC. The total increase in porosity observed with extraction correlated well with the amount of S2 determined by the SRA pyrolysis.

No shift was observed in the pore size distributions in any extracted samples, suggesting Mechanisms 1 and 2 dominate Mechanism 3. To understand the effect of various solvents on different pore size ranges, the SANS data were partitioned into five ranges. For each of the solvents tested, the change in porosity observed was consistent across ranges 3 through 5 (8.91 nm – 1.35 μm). However, in MAR HM and CARB LM, contact with acetone and methanol increased porosity dramatically in range 5 (272 nm – 1.35 μm) compared to the other ranges.

This suggests native organics compatible with methanol and acetone are contained within this pore size range. In addition, complex fluid-rock interactions, such as swelling of the matrix by the solvents, appear to have occurred. These were particularly apparent in the low-maturity clay-rich sample. Additionally, this study showed that the amount of extractable material, paraffinic hydrocarbons (<C28), could not be directly correlated to the changes in porosity measured by SANS.

Assuming that the results obtained have some generality beyond the few samples tested, the data may have significant implications both for understanding the distribution of organics in tight oil/gas shales as a function of pore size, and for examining the effect of organic solvents on pore structure. If certain solvents cause swelling in shales and decrease conductivity they may reduce, rather than enhance recovery. These determinations of structure of pores in shales, including swelling, can inform numerical models for hydrocarbon diffusion, migration, and extraction. The location and nature of organic/inorganic interfaces between organic matter and surrounding minerals may also play an important role in transport.(Collell et al., 2015)

This study has demonstrated that exposure to organic solvents causes complex physical and chemical interactions in shales, not only simple dissolution of native organic matter. SANS results have shown these interactions could include clay swelling, breakdown, dissolution, or migration of resins and asphaltenes. Additionally, important pore size ranges have been identified in shales which respond differently to solvents. Large pores (> 270 nm) have been recognized in certain shales as containing asphaltenes and resins with polar groups. Clays have also been seen to play a significant role in hydrocarbon extraction and porosity, especially in the Eagle Ford shale. The amount of extractable paraffinic hydrocarbons (< C28) has been related to the fraction of clay minerals present. These hydrocarbons may be stored in the small pore size

range (< 8.9 nm) within clays identified by SANS. Thus, this study has demonstrated important relationships in how native organics are distributed within the pore structure of shales.

AUTHOR INFORMATION

Corresponding Author

*Victoria DiStefano, Oak Ridge National Laboratory, 1 Bethel Valley Road, Oak Ridge, TN 37831, distefanovh@ornl.gov

Author Contributions

The manuscript was written through contributions of all authors. All authors have given approval to the final version of the manuscript. The authors contributed equally.

Funding Sources

Funding for the project came from the US Department of Energy through the following programs: Research Partnership to Secure Energy for America, Office of Science, Scientific User Facilities Program, and from Laboratory Directed Research and Development of Oak Ridge National Laboratory, managed by UT-Battelle. The University of Tennessee supported the research through the Bredesen Center. Chesapeake Energy also supported the research.

Notes

The authors declare no competing financial interest.

ACKNOWLEDGMENTS

J.M. funding came from the Research Partnership to Secure Energy for America, contract NFE-11-03260. AGS and ADG research sponsored by the Laboratory Directed Research and Development Program of Oak Ridge National Laboratory, managed by UT-Battelle, L.L.C., for the U. S. Department of Energy. V.H.D. and L.M.A. were supported by the U.S. Department of

Energy, Office of Science, Basic Energy Sciences, Chemical Sciences, Geosciences, and Biosciences Division. V.H.D. also thanks the Bredesen Center at the University of Tennessee in Knoxville for support. A portion of this research at ORNL's High Flux Isotope Reactor was sponsored by the Scientific User Facilities Division, Office of Basic Energy Sciences, U.S. Department of Energy. The authors would like to thank Michael Cheshire for many discussions about the effect of clays on the SANS data.

ABBREVIATIONS

DTA, differential thermal analysis; GC-MS, gas chromatography-mass spectrometry; HFIR, high flux isotope reactor; HI, hydrogen index; HP, Hewlett Packard; m/z, mass-to-charge ratio, OI, oxygen index; R_0, thermal maturity or vitrinic reflectance; RT, retention time; SANS, small angle neutron scattering; SAXS, small angle X-ray scattering; SEM, scanning electron microscopy; SRA, source rock analyzer; TGA, thermogravimetric analysis; TOC, total organic carbon; UHP, ultra-high purity; USANS, ultra-small angle neutron scattering; USAXS, ultra-small X-ray scattering

Graphical Abstract

This research comprises a multidisciplinary study showcasing the use of neutron scattering to understand changes in shale porosity arising from hydrocarbon extraction. The shales were analyzed using standard rock evaluation methods, and hydrocarbons were extracted by leaching with a variety of organic solvents. The pore size distribution was probed using small angle neutron scattering. Most of the shale samples came from the Eagle Ford play in Texas, but we also obtained samples from the Marcellus play in Pennsylvania. There are three possible mechanisms of porosity development due to extraction by solvents that could be observed by SANS. Porous kerogen and bitumen in the rock matrix (composed of minerals and nonporous or inaccessible porous kerogen) could (1) completely breakdown into smaller molecules that can be extracted (2) migrate into smaller pores or (3) partially dissolve leaving behind the kerogen portion. This study can serve as a demonstration of how neutron scattering, along with other methods of analysis, can be used to understand complex fluid (fuel)-rock interactions in geological samples.

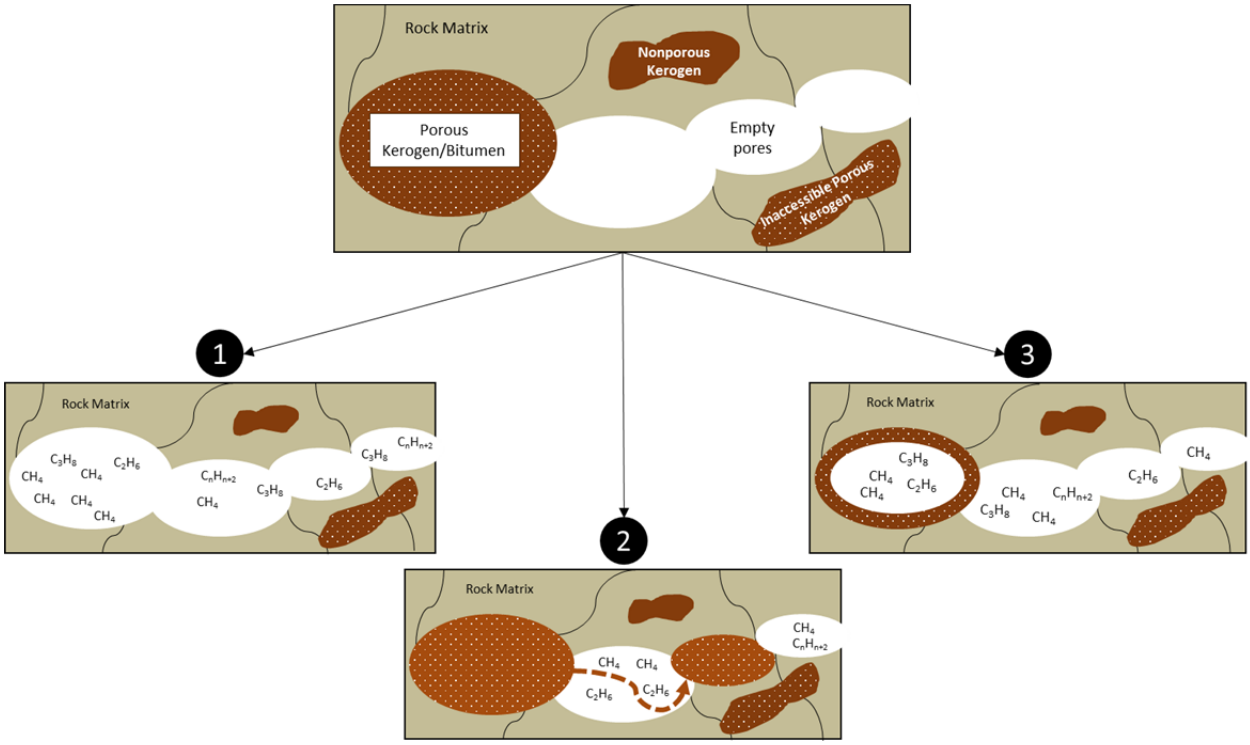

REFERENCES

Ambrose, R. J., Hartman, R. C., Diaz-Campos, M., Akkutlu, I. Y., Sondergeld, C. H., and doi:, P., 2010. New pore-scale considerations for shale gas in place calculations*Soc. Pet. Eng. Unconv. Gas Conf.*, Pittsburgh, PA.

Anovitz, L. M. and Cole, D. R., 2015. Characterization and analysis of porosity and pore structures. *Rev. Mineral. Geochem.* **80**, 61-164.

Anovitz, L. M., Cole, D. R., Rother, G., Allard, L. F. J., Jackson, A., and Littrell, K. C., 2013. Diagenetic changes in macro-to nano-scale porosity in the St. Peter Sandstone: an (Ultra) small angle neutron scattering and backscattered electron imaging analysis. *Geochimica et Cosmochimica Acta* **102**, 280-305.

Anovitz, L. M., Cole, D. R., Sheets, J. M., Swift, A., Elston, H. W., Welch, S. A., Chipera, S. J., Littrell, K. C., Mildner, D. F. R., and Wasbrough, M. J., 2015. Effects of maturation on multiscale (nanometer to millimeter) porosity in the Eagle Ford shale. *Interpretation* **5**, SU59-SU70.

Anovitz, L. M., Lynn, G. W., R., C. D., Rother, R., Allard, L. F., Hamilton, W. A., Porcar, L., and Kim, M.-H., 2009. A new approach to quantification of metamorphism using ultrasmall and small angle neutron scattering. *Geochimica et Cosmochimica Acta* **73**, 7303-7324.

Aylmore, L. A. G. and Quirk, J. P., 1971. Domains and quasi-crystalline regions in clay systems. *Soil Sci Soc of Am J* **35**, 652-654.

Bahadur, J., Radliński, A. P., Melnichencko, Y. B., Mastalerz, M., and Schimmelmann, A., 2015. Small-angle and ultrasmall-angle neutron scattering (SANS/USANS) study of New Albany shale: A treatise on microporosity. *Energy and Fuels* **29**, 567-576.

Ballice, L. and Larsen, J. W., 2003. Changes in the cross-link density of Goynuk oil shale (Turkey) on pyrolysis. *Fuel* **82**, 1305-1310.

Barton, C. J., 1983. *Handbook of Solubility Parameters*. CRC Press.

Bernard, S. and Horsfield, B., 2014. Thermal maturation of gas shale systems. *Annu Rev Earth Planet Sci* **42**, 635-651.

Bernard, S., Horsfield, B., Schulz, H. M., Wirth, R., Schreiber, A., and Sherwood, N., 2012a. Geochemical evolution of organic-rich shales with increasing maturity: a STXM and TEM study of the Posidonia Shale (Lower Toarcian, northern Germany). *Mar. Pet. Geol.* **31**, 70–89.

Bernard, S., Wirth, R., Schreiber, A., Schulz, H. M., and Horsfield, B., 2012b. Formation of nanoporous pyrobitumen residues during maturation of the Barnett Shale (FortWorth Basin). *Int. J. Coal Geol.* **10**, 3-11.

Cases, J. M., Berend, I., Besson, G., Francois, M., Uriot, J. P., Thomas, F., and Poirier, J. E., 1992. Mechanism of adsorption and desorption of water vapor by homoionic montmorillonite. 1. The sodium-exchanged form. *Langmuir* **8**, 2730-2739.

Cervini-Silva, J., 2004. Coupled hydrophilic and charge-transfer interactions between polychlorinated methanes, ethanes, and ethenes and redox-manipulated smectite clay minerals. *Langmuir* **20**, 9878-9881.

Chen, C., Hu, D., Westacott, D., and Loveless, D., 2013. Nanometer-scale characterization of microscopic pores in shale kerogen by image analysis and pore-scale modeling. *Geochemistry Geophysics Geosystems* **14**, 4066-4075.

Clarkson, C. R., Solano, N., Bustin, R. M., Bustin, A. M. M., Chlmers, G. R. L., He, L., Melnichencko, Y. B., Radliński, A. P., and Blach, T. P., 2013. Pore structure characterization of North American shale gas reservoirs using USANS/SANS, gas adsorption, and mecury intrusion. *Fuel* **103**, 606-616.

Collell, J., Galliero, G., Vermorel, R., Ungerer, P., Yiannourakou, M., Montel, F., and Pujol, M., 2015. Transport of multicomponent hydrocarbon mixtures in shale organic matter by molecular simulations. *J Phys Chem C* **119**, 22587-22595.

Curtis, M. E., Ambrose, R. J., and Sondergeld, C. H., 2010. Structrual characterization of gas smales on the micro- and nano-scales*Canadian Unconventional Resources and International Petroleum Conference*. Society of Petroleum Engineers, Calgary, AB.

Ge, X., Fan, Y., Cao, Y., Li, J., Cia, J., Liu, J., and Wei, S., 2016. Investigation of organic related pores in unconventional reservoir and its quantitative evaluation. *Energy and Fuels* **30**, 4699-4709.

Glatter, O. and Kratky, O., 1982. Small Angle X-ray Scattering. Academic Press, London.

Graber, E. R. and Mingelgrin, U., 1994. Clay swelling and regular solution theory. *Environmental Science & Technology* **28**, 2360-2365.

Gu, X., Cole, D. R., Rother, G., Mildner, D. F. R., and Brantley, S. L., 2015. Pores in Marcellus shale: A neutron scattering and FIB-SEM study. *Energy and Fuels* **29**, 1295-1308.

Hall, P. L., Mildner, D. F. R., and Borst, R. L., 1986. Small-angle scattering studies of the pore spaces of shaly rocks. *J Geophysical Research* **91**, 2183-2192.

Huc, A.-Y., 2013. *Geochemistry of fossil fuels: from conventional to unconventional hydrocarbon systems*. Editions Technip.

Job, N., Thery, A., Pirard, R., Marien, J., Kocon, L., Rouzaud, J.-N., Beguin, F., and Pirard, J.-P., 2005. Carbon aerogels, cryogels and xerogels: Influence of the drying method on the textural properties of porous carbon materials. *Carbon* **43**, 2481-2494.

Jones, T. R., 1983. The properties and uses of clays which swell in organic solvents. *Clay Minerals* **18**, 399-410.

Kabiri, K. and Zohuriaan-Mehr, M. J., 2004. Porous superabsorbent hydrogel composites: Synthesis, morphology, and swelling rate. *Macromol. Mater.Eng.* **289**, 635-661.

Kemp, W., 1981. *Organic Spectroscopy*. The Macmillan Press Ltd, London, Great Britain.

Koel, M., Ljovin, S., Hollis, K., and Rubin, J., 2001. *Pure and Applied Chemistry* **73**.

Kowalska, M., Guler, H., and Cocke, D. L., 1994. Interactions of clay minerals with organic pollutants. *The Science of the Total Environment* **141**, 223-240.

Kuila, U., McCarty, D. K., Derkowski, A., Fischer, T. B., and Prasad, M., 2014. Total porosity measurement in gas shales by the water immersion porosimetry (WIP) method. *Fuel* **117**, 1115-1129.

Kuila, U. and Prasad, M., 2013. Specific surface area and pore-size distribution in clays and shales. *Geophysical Prospecting* **61**, 341-362.

Kuila, U., Prasad, M., Derkowski, A., and McCarty, D. K., 2012. Compositional controls on mudrock pore-size distribution: An example from Nibrara formation*SPE Annual Technical Conference and Exhibition*. Society of Petroleum Engineers, San Antonio, TX.

Lagaly, G., 1984. Clay-organic interactions. *Phil Trans R Soc London A* **311**, 315-332.

Lee, S., Fischer, T. B., Stokes, M. R., Klingler, R. J., Ilavsky, J., McCarty, D. K., Wignad, M. O., Derkowski, A., and Winans, R. E., 2014. Dehydration effect on the pore size, porosity, and fractal parameters of shale rocks: Ultrasmall-angle X-ray scattering study. *Energy and Fuels* **28**, 6772-6779.

Loucks, R. G., Reed, R. M., Ruppel, S. C., and Jarvie, D. M., 2009. Morphology, genesis, and distribution of nanometer-scale pores in siliceous mudstones of the Mississippian Barnett shale. *J. Sedimentary Res* **79**, 848-861.

Mastalerz, M., Schimmelmann, A., Drobniak, A., and Chen, Y., 2013. Porosit of Devonian and Mississippian New Albany shale across a maturation gradient: Insights from organic petrology, gas adsorption, and mercury intrusion. *AAPG Bulletin* **97**, 1621-1643.

McCarthy, K., Rojas, K., Niemann, M., Palmowski, D., Peters, K., and Stankiewicz, A., 2011. *Oilfield Review* **23**.

Neaman, A., Pelletier, M., and Villieras, F., 2003. The effects of exchanged cation, compression, heating and hydrationon textural properties of bulk bentonite and its corresponding purified montmorillonite. *Applied Clay Science* **22**, 153-168.

Radke, M., Sittardt, H. G., and Welte, D. H., 1978. Removal of soluble organic matter from rock samples with a flow-through extraction cell. *Anal Chem* **50**, 663-665.

Radliński, A. P., 2006. Small-angle neutron scattering and rock microstructure. *Reviews in Mineralogy and Geochemistry* **Neutron Scattering in Earth Sciences**, 363-397.

Radliński, A. P., Boreham, C. J., Lindner, P., Randl, O., Wignall, G. D., Hinde, A., and Hope, J. M., 2000. Small angle neutron scattering signature of oil generation in artificially and naturally matured hydrocarbon source rocks. *Organic Geochemistry* **31**, 1-14.

Radliński, A. P. and Hinde, A. L., 2002. Small angle neutron scattering and petrolem geology. *Neutron News* **13**, 10-14.

Radliński, A. P., Ioannidis, M. A., Hinde, A. L., Hainbuchner, M., Baron, M., Rauch, H., and Kline, S. R., 2004. Angstrom-to-millimeter characterization of sedimentary rock microstructure. *J. Colloid Interface Sci* **274**, 607-612.

Rodriguez, R., Crandall, D., Song, X., Verba, C., and Seoder, D., 2014. Imaging Techniques for Analyzing Share Pores and Minerals. National Energy Technology Laboratory, Morgantown, WV.

Rother, G., Melnichencko, Y. B., Cole, D. R., Freilinghaus, H., and Wignall, G. D., 2007. Microstructural characterization of adsorption and depletion regimes of supercritical fluids in nanopores. *J Phys Chem C* **111**, 15736-15742.

Saliger, R., Bock, V., Petricevic, P., Tillotson, T., Geis, S., and Fricke, J., 1997. Carbon aerogels from dilute catalysis of resorcinol with formaldehyde. *J. Non-Crystal. Solids* **221**, 144-150.

Sing, K. S. W., Everett, D. H., Haul, R. A. W., Moscou, L., Pierotti, R. A., Rouqerol, J., and Siemieniewska, T., 1985. Reporting physisorption data for gas/solid systems. *Pure and Applied Chemistry* **57**, 603-619.

Sondergeld, C. H., Ambrose, R. J., Rai, C. S., and Moncreiff, J., 2010. Micro-structural studies of gas shales*SPE Unconventional Gas Conference*. Society of Petroleum Engineers, Pittsburgh, PA.

Stack, A. G., 2015. Precipitation in pores: A geochemical frontier. *Rev. Mineral. Geochem.* **80**, 165-190.

Swainson, I. P., 2015. Pore-Scale Geochemical Processes*Reviews in Mineralogy & Geochemistry*. Mineralogical Society of America, McLean VA.

Swift, A. M., Anovitz, L. M., Sheets, J. M., Cole, D. R., Welch, S. A., and Rother, G., 2014. Relationship between mineralogy and porosity in seals relevant to geologic CO_2 sequestration. *Environ. Geosci.* **21**, 39-57.

Wang, H.-W., Anovitz, L. M., Burg, A., Cole, D. R., Allard, L. F., Jackson, A. J., Stack, A. G., and Rother, G., 2013. Multi-scale characterization of pore evolution in a combustion metamorphic complex, Hatrurim basin, Israel: Combining (ultra) small-angle neutron scattering and image analysis. *Geochim et Cosmochim Acta* **121**, 339-362.

Wang, H., Wang, X., Jin, X., and Cao, D., 2016. Molecular dynamics simulation of diffusion of shale oils in montmorillonite. *J Phys Chem C* **120**, 8986-8991.

Warren, D. S., Clark, A. I., and Perry, R., 1986. A review of clay-aromatic interactions with a view to their use in hazardous waste disposal. *The Science of the Total Environment* **54**, 157-172.

Webber, J. B. W., Corbett, P., Semple, K. T., Ogbonnaya, U., Teel, W. S., Masiello, C. A., Fisher, Q. J., Valenza, J. J. I., Song, Y.-Q., and Hu, Q., 2013. An NMR study of porous rock and biochar containing organic material. *Microporous and Mesoporous Materials* **178**, 94-98.

Weng, X., 2015. Modeling of complex hydraulic fractures in naturally fractured formation. *J Unconventional Oil and Gas Resources* **9**, 114-135.

Wignall, G. D., Littrell, K. C., Heller, W. T., Melnichencko, Y. B., Bailey, K. M., Lynn, G. W., Myles, D. A., Urban, V. S., Buchanan, M. V., Selby, D. L., and Butler, P. D., 2012. The 40 m general purpose small-angle neutron scattering instrument at Oak Ridge National Laboratory. *J Appl Cryst* **45**, 990-998.

Yariv, S., 1996. Thermo-IR-spectroscopy analaysis of the interactions bewteen organic pollutants and clay minerals. *Thermochim. Acta* **274**, 1-35.